

Mapping deciduous forest ice storm damage using Landsat and environmental data

Ian Olthof^{a,*}, Douglas J. King^a, R.A. Lautenschlager^b

^aDepartment of Geography and Environmental Studies, Carleton University, 1125 Colonel By Drive, Ottawa, Ontario, Canada K1S 5B6

^bAtlantic Canada Conservation Data Centre, P.O. Box 6416, Sackville, New Brunswick, Canada E4L 1G6

Received 23 May 2003; received in revised form 3 October 2003; accepted 10 November 2003

Abstract

Sugar maple (*Acer Saccharum Marsh.*) damage resulting from a severe ice storm was modeled and mapped over eastern Ontario using pre- and post-storm Landsat 5 imagery and environmental data. Visual damage estimates in 104 plots and corresponding reflectance and environmental data were divided into multiple, mutually exclusive training and reference datasets for damage classification evaluation. Damage classification accuracy was compared among four methods: multiple regression, linear discriminant analysis, maximum likelihood, and neural networks. Using the best classifier, various stratification methods were assessed for potential inflationary effects on classification accuracy due to spatial proximity between training and reference data. Of the classifiers that were evaluated, neural networks performed best. Neural networks 'learn' training data accurately (94% overall), but classify proximate reference data less accurately (65%), and distant, spatially independent reference data least accurately (55%). Results indicate that, while remotely sensed and environmental data cannot discriminate among many levels of deciduous ice storm damage, they can be considered useful for differentiating areas of low to medium damage from areas of severe damage (69% accuracy). Such classification methods can provide regional damage maps more objectively than point-based visual estimates or aerial sketch mapping and aid in identification of areas of severe damage where management intervention may be advantageous.

© 2003 Elsevier Inc. All rights reserved.

Keywords: Ice storm; Forest damage; Classification; Accuracy assessment

1. Introduction

Ice storms are a major recurring regional scale disturbance (Lemon, 1961) responsible for tree mortality in temperate hardwood forests (Hauer et al., 1994; McKay & Thomson, 1969). From January 4th to the 10th, 1998, between 40 and 100 mm of freezing rain fell across eastern Ontario, southern Quebec, and the northeast United States, leading to one of the most severe ice storms in the region's history. The maple syrup industry, which contributes \$11 million annually to the regional economy of eastern Ontario (Kidon et al., 2001), was devastated. Compensation was provided to maple syrup producers for cleanup and for expected losses to maple syrup production during the period of forest recovery. Due to the unprecedented nature of the

event, methods for accurate regional-scale damage assessment did not exist, nor was the required time for full recovery known. Most damage assessment for compensation was conducted based on site visits and aerial sketch mapping (Scarr et al., 2003). More objective and spatially explicit means of mapping ice storm damage were needed to help understand the effects of this storm and to provide a baseline from which forest recovery could be monitored.

Remote sensing has a potential role in damage mapping because it can provide spatially explicit vegetation reflectance change due to disturbance. In particular, archived imagery such as Landsat may enable pre- and post-storm change analysis. Additional environmental information from topography or meteorology data may be combined with remotely sensed imagery to model and map damage regionally.

This paper compares four classification methods using available geospatial data to map forest ice storm damage across eastern Ontario. In this process, classification accuracies are presented for conventional statistical and neural

* Corresponding author.

E-mail addresses: iolthof@ccs.carleton.ca (I. Olthof), doug_king@carleton.ca (D.J. King).

network classifiers. Classification accuracy is also compared for different stratifications of available plot and block data to determine the range of classification accuracies, and to evaluate the potential inflationary effects of spatially proximal training and test data.

1.1. Effects of damage on canopy reflectance

Forest damage results in altered forest structure from either: (1) biotic or abiotic stress agents such as insects, disease, and pollution; or (2) sudden catastrophic events such as fire or severe weather. Structural changes can occur at scales from individual leaves to forest canopies (Mageau et al., 1995), depending on the spatial and temporal extent of the damaging event. Sudden catastrophic disturbances such as wind or ice storms result in immediate forest canopy damage from broken branches and toppled trees.

Certain generalizations can be made about the image expression of forest damage. These assume that canopy closure is high prior to the disturbance event so that the remote sensing signal is produced by illuminated crowns and shadowed gaps. Where the canopy is relatively sparse and the ground is illuminated, the effects of damage on image expression are subtler and these generalizations may not hold. Forest structure has been shown to be the main determinant of above canopy reflectance over a wide range of conditions (Treitz & Howarth, 1996), while leaf reflectance also contributes.

An undamaged forest canopy seen from above will have a characteristic shadow fraction and brightness related to the canopy gap fraction and distribution. With increasing levels of damage, the canopy becomes more irregular as branches break and entire trees topple. The irregular structural configuration that results from damage manifests itself as increased image shadow due to a higher gap fraction and increased mutual shading, generally contributing to lower canopy reflectance. Lower reflectance is also caused by a decrease in canopy biomass, particularly in the green peak and NIR plateau.

At high levels of damage, the signal often becomes brighter as gap frequency and size increase and the understory or forest floor becomes illuminated. This effect is especially pronounced at the ‘hot spot’ where the observation and illumination directions coincide within the same canopy gap (Chen & Leblanc, 1997). An inverse relationship between spectral response produced by a larger gap fraction and gap brightness (Seed & King, 2003) may offset each other when measuring overall canopy reflectance. Increased brightness at high levels of damage may also be caused by greater direct scattering from damaged and irregular canopy surfaces. These two structural effects, in addition to stress factors that produce increased visible reflectance at the leaf level (OMNR, 1997), have led many authors to report increasing visible, NIR, and mid-IR reflectance with higher levels of canopy damage (Ardo et al., 1997; Radeloff et al., 1999).

This trend has consistently been observed in conifers due their low reflectance in undamaged conditions and generally deciduous understory (Radeloff et al., 1999).

Vegetation stress may also produce changes in the typical reflectance curve of healthy leaves. Stress generally leads to a decrease in total chlorophyll content and a change in the proportion of light absorbing pigments, causing less overall absorption in the visible bands (OMNR, 1997). These changes have consistently produced greater reflectance in the green peak centred at 570 nm (Collins, 1978; Gates et al., 1965; Horler et al., 1980) and in the red chlorophyll absorption band (Lillesand & Kiefer, 1999). The result of an increase in both green and red reflectance is visible yellowing of stressed or damaged leaves. A shift in the red edge has also consistently been reported, though some authors have reported a shift towards shorter wavelengths, while others have reported a shift towards longer wavelengths (Singhroy, 1995). NIR reflectance is relatively insensitive to plant stress, but sensitivity increases in the mid-IR from 1400 to 2500 nm due to severe leaf dehydration and the accompanying decreased absorption by water (Carter, 1993; Rock et al., 1989). The structural and leaf reflectance effects described above may combine to produce either a non-linear relation or a low sensitivity of reflectance to damage.

1.2. Forest damage mapping using remotely sensed imagery

Forest damage modeling and mapping studies have applied various methods, including linear regression (Collins & Woodcock, 1996; Franklin et al., 1995) and stepwise linear regression (Ekstrand, 1994), logit regression (Lambert et al., 1995), discriminant analysis (Franklin et al., 1995), supervised and unsupervised classification (Franklin et al., 1995), and neural networks (Ardo et al., 1997). Multi-temporal imagery has been used to establish a pre-disturbance baseline from which damage can be measured (Ardo et al., 1997; Collins & Woodcock, 1996; Ekstrand, 1994; Franklin et al., 1995; Radeloff et al., 1999). Collins and Woodcock (1996) assessed three linear change detection techniques for mapping forest mortality, including multi-temporal principal components analysis. Additional image processing techniques worth noting include the use of band ratios (e.g., Vogelmann, 1990) and spectral unmixing (Radeloff et al., 1999). Other studies have included topographic data to improve damage prediction (Ardo et al., 1997).

Most previous damage mapping studies have assessed defoliation in conifer forests (Ardo et al., 1997; Collins & Woodcock, 1996; Franklin et al., 1995; Lambert et al., 1995; Radeloff et al., 1999; Vogelmann, 1990). Deciduous forest damage has been modeled using high-resolution airborne imagery (Lévesque & King, 2003; Olthof & King, 2000; Pellikka et al., 2000; Yuan et al., 1991),

and in a few studies, satellite imagery (Ekstrand, 1994; Vogelmann, 1990; Vogelmann & Rock, 1989) for mixed forest damage assessment.

Vogelmann and Rock (1989) mapped deciduous forest damage with Landsat Thematic Mapper (TM) data using visual assessment of spectral bands, band ratios and multi-temporal image differencing. Specifically, they sought to distinguish between defoliated and non-defoliated sites using RGB images consisting of a Landsat TM5/4 band ratio, TM band 5, and TM band 3 as red, green, and blue, respectively. Additionally, a pre–post damage difference image of TM band 4 was combined with TM bands 5 and 3 in an RGB composite image. *T*-tests were used to verify the discriminating ability between 10 defoliated and 10 non-defoliated sites of the TM5/4 ratio and the TM4 difference image. Resulting composite maps were visually compared to aerial sketch maps, and the level of agreement between them was found to be quite good.

Vogelmann (1990) discriminated high, medium, and low levels of deciduous forest damage using two separate vegetation indices, including a TM5/4 ratio and the normalized difference vegetation index ($NDVI = (TM4 - TM3) / (TM4 + TM3)$). Vegetation indices from 12 non-defoliated and 14 defoliated sites were compared using *t*-tests. The TM5/4 ratio was able to distinguish between high and low damage areas, but it did not appear to be able to discriminate between medium and low damage. The *t*-test for NDVI confirmed its ability to distinguish high, medium, and low damage areas.

Results vary among these studies due to the numerous methods used, scales of assessment, damage measures, image quality, and pre-processing. An additional source of variation in classification error is associated with training and reference site selection. For example, Friedl et al. (2000) stratified ground data into five mutually exclusive training and reference sets generated randomly in an 80% to 20% ratio to examine bias effects on the accuracy assessment of AVHRR land cover maps. By using multiple cross-validations, they showed that classification accuracy varies due to the effects of spatial autocorrelation between training and reference data. Spatial autocorrelation implies a relation between two attributes in space whose similarity decreases with increasing distance. Plots used to train a classifier and those used as reference data to test its accuracy may be similar due to spatial proximity, thereby violating the assumption of independence between training and reference data that is necessary for proper validation.

In the study presented here, 37 blocks, each consisting of four treatment plots and assessed independently for damage caused by the ice storm, were established by the Ontario Ministry of Natural Resources (OMNR) in sugar maple (*Acer Saccharum Marsh.*) bushes located across eastern Ontario (Lautenschlager & Nielsen, 1999) (Fig. 1). Each block was 100 m on a side and was divided into four 50×50 m plots. While this design was intended to allow comparisons of plot treatments within each block, it also enabled assessment of the effects of spatial proximity

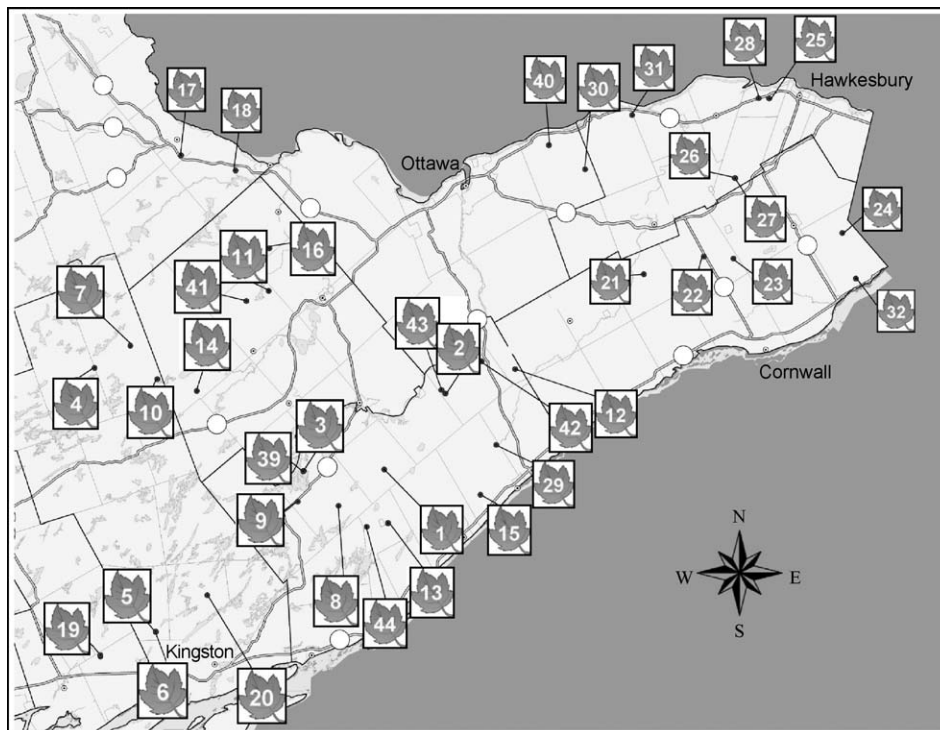


Fig. 1. Block locations and numbers in productive sugar bushes, across southeastern Ontario.

between training and validation data on classification accuracy.

1.3. Objectives

The primary objective of this study was to compare four classification methods for ice storm forest damage mapping. The methods were: linear stepwise regression, linear discriminant analysis, maximum likelihood, and neural networks. A second objective was to determine remote sensing and environmental variables that can be effectively used to predict and map damage. The third objective was to analyze and compare classification accuracies obtained using three reference datasets: the training data, reference data samples located in close proximity to the training samples, and reference data that were spatially independent of the training data.

2. Data acquisition and processing

2.1. Forest damage data

The OMNR provided plot-based visual damage estimates (mean percent crown loss for 6 representative focus trees per plot; 24 per block) acquired in the fall of 1998. Individual tree estimates of crown loss were unavailable for 3 blocks (blocks 39, 41, and 44), leaving 34 blocks, or 136 plots for this analysis. In this study, modelling is conducted using these continuous damage data and classification is conducted using pre-determined damage classes. The average percent crown loss of the six focus trees was assigned to low (0–25%), medium (26–50%), and high (51%+) damage classes for classification purposes. These class divisions were selected to be able to assign a probability of mortality based on existing literature. Both low and medium damage classes have a high to moderate chance of survival depending on tree vigour prior to the event, while the high damage class represents varying probabilities of survival from moderate to low with expected internal infection and/or growth suppression (Coons, 1999; QMNR, 2000). These classes were also selected because they were in common use in other ice storm studies.

2.2. Environmental data

In order to map forest damage, a geospatial dataset consisting of environmental data and satellite multispectral imagery was assembled. Environmental data consisted of elevation, slope, and aspect, total freezing precipitation, and proximity to forest edge. These variables were selected as likely candidates for prediction of damage based on their representation of exposure (e.g., dominant wind direction was from the northeast) (Milton & Bourque, 1999) and ice accumulation (Proulx & Greene,

2001). Satellite data consisted of pre- and post-ice storm Landsat 5 TM spectral bands 1–5 and 7 from the visible to the mid-IR. These data were used as independent variables to predict and map damage as the dependent variable. Each data type is described in more detail below.

2.2.1. Elevation, slope, and aspect

Elevation data available for 116 of the 136 plots were extracted from the Ontario Base Mapping (OBM) Digital Topographic Data Base (DTDB) of eastern Ontario. The data were provided by the OMNR as an interpolated surface of 50-m cells derived from a 50-m grid of spot heights that had been measured photogrammetrically from 1:10,000 airphotos. Slope and aspect variables were derived from the elevation surface using standard GIS software.

2.2.2. Freezing rain

Total freezing rain equivalent data were provided by Environment Canada for 284 weather stations in the ice-affected region where rain measurements had been made hourly or twice daily during the storm. A freezing rain surface was generated with a 30-m cell size through kriging interpolation of point estimates using a spherical fit.

2.2.3. Forest classification

In the study region, forests are composed primarily of deciduous species with smaller areas of coniferous or mixed species. For the purposes of this study, damage classification was conducted for deciduous forests only, as damage data for coniferous and mixed forests did not exist in the same format as described above, and the primary application of the map was for sugar maple damage assessment. Land cover information was obtained from two sources of data. The OMNR Ontario Base Map data layer ‘Woodarea’, which was derived from interpreted 1991 1:10,000 aerial photography, consisted of a vector representation of woodland boundaries. In order to extract only deciduous forest areas, these woodland forest polygons were overlaid onto a thematic land cover map derived from clustering using Classification by Generalized Progression (CPG) classification (Latifovic et al., 1999) of a mosaic of four post-storm Landsat TM scenes (see below). CPG is an unsupervised classification that forms clusters using both spectral and spatial similarity criteria. The thematic map classification included separate deciduous and coniferous classes.

In the TM map, coniferous forest was originally classified with a 78.8% user’s accuracy (100% – % errors of commission) using TM data only and independent reference areas that were visually interpreted from 60-cm pixel airborne digital camera imagery. Once the TM classification was combined with the ‘Woodarea’ layer, confusion between conifer, water, and agricultural crop classes was eliminated, increasing the conifer classification accuracy to 97.0%. Similarly, deciduous classification accuracy increased from 59.0% in the CPG map to 91.0% after

intersection of the two spatial datasets. In addition to focusing damage classification on deciduous forests only, the map was also used to calculate proximity of forest pixels to the closest forest edge.

Though it was desirable to further stratify forest cover to account for differential susceptibility of species to ice storm damage (Hopkin et al., 2003), no species cover data existed at the time of this study, nor were there accurately positioned field plots in all forest types. Since this study, the OMNR has been in the process of updating its Forest Resource Inventory (FRI) of eastern Ontario, which should provide species composition and allow additional stratification of forest types for future mapping.

2.3. Remote sensing data: Landsat TM

Eight TM scenes were used to generate two separate mosaics—one pre- and the other post-ice storm. The best scenes available with the desired coverage were selected based on a report of scene quality and on visual assessment of cloud cover. Given the limitations of data availability primarily due to cloud cover, pre-storm data consisted of scenes acquired in July of 1996 and 1997, while post-storm scenes were acquired in August and September of 1998 and July 1999 (Table 1). The 1999 scene was generated by the Landsat 7 Enhanced Thematic Mapper (ETM+), which has somewhat different radiometric characteristics than the Landsat 5 TM sensor of the other scenes. There were, however, only three study blocks contained within it.

Georeferencing was accomplished to sub-pixel positional accuracy in a series of steps using airborne digital camera imagery of the maple blocks as an intermediate data source between differential GPS surveyed ground targets and Landsat imagery. Relative radiometric calibration was performed by plotting radiance in overlap areas between scenes to

determine the linear function relating stable land elements in adjacent or multi-temporal scene pairs. A single scene located closest to an Aerocan sun tracking photometer station (Holben et al., 1998) was selected as the master to which all other scenes were relatively calibrated. Once a mosaic covering Eastern Ontario was produced, absolute calibration to surface reflectance was performed by applying aerosol optical depth data from the Aerocan photometer, and sensor gains and offsets from the master to the whole mosaic. Gain and offset information from the master scene and aerosol optical depth data were entered into the calibration program 6S (Vermote et al., 1997) to convert scene radiance to surface reflectance for each of the six TM bands (TM1–5 and 7).

Landsat image variables used in damage classification included pre- and post-storm reflectance in six bands and NDVI, as well as ratios of pre-/post-storm TM bands and NDVI. Single pixels that fell entirely within plot boundaries were used to represent plot reflectance.

3. Methods of classification of ice storm damage and stratification of training and reference data

Forest damage was first modelled as a continuous variable using linear stepwise regression. Subsequently, using the three damage classes, four classifiers were implemented and compared: classification of the linear regression continuous function, linear discriminant analysis, maximum likelihood, and a neural network.

For the parametric methods (regression, discriminant analysis, and maximum likelihood), histograms were visually checked for normality and transformations were applied to non-normal data in an attempt to normalize their distributions. The spectral bands, band ratios and NDVI, elevation, and precipitation were determined to be sufficiently normal for input into parametric models. Aspect could not be included as an independent variable in the parametric models due to its circular nature. Slope was highly related to elevation in the study area ($r=0.43$, $P<0.01$) and could not be transformed to a normal distribution. A logarithmic transformation was applied to proximity to forest edge to normalize its distribution.

3.1. Modeling and classification methods

3.1.1. Linear regression

In modelling of damage as a continuous variable, forward stepwise linear regression was performed 100 different times (trials) using samples drawn from the 104 plots as shown in Table 2. Probabilities to enter and remove were set at 0.05 and 0.10, respectively. The resulting models consisted of between two and six significant predictive variables. As models consisting of certain groups of variables were generated more frequently than others, a comparative analysis of prediction errors

Table 1
Pre and post 1998 ice storm Landsat scenes selected for forest damage mapping

Path	Row	Sensor	Date and time of acquisition	Scene centre
15	28	TM	July 30, 1997, 15:15:21	529812.177 E, 5098447.555 N
15	29	TM	July 30, 1997, 15:15:46	489003.780 E, 4959470.205 N
16	28	TM	July 18, 1996, 15:04:59	416822.886 E, 5099703.094 N
16	29	TM	July 18, 1996, 15:05:23	380581.208 E, 4962369.540 N
15	28	TM	August 2, 1998, 15:22:43	529812.177 E, 5098447.555 N
15	29	TM	August 2, 1998, 15:23:07	489003.780 E, 4959470.205 N
16	28	ETM+	July 3, 1999, 15:43:22	416822.886 E, 5099703.094 N
16	29	TM	September 10, 1998, 15:29:40	380581.208 E, 4962369.540 N

Table 2
Samples used in different phases of damage modeling and classification error analyses

Phase/application	1	2 ^a	3 ^a	4
	Examine regression errors and variable reduction	Comparison among classifiers	Assess NN accuracy distribution from set 2	Assess NN accuracy using block-based stratification
Damage variable	Continuous	Ordinal		
Stratification	Plot	Plot	Plot	Block
Method				
Regress	x	x		
Discrim		x		
Max likelihood		x		
NN		x	x	x
# cross-validation trials	100	10	10	20
# training plots/trial	80	80	80	84
# reference plots/trial	24	24	24	20

^a Subsets extracted from set 1.

between these model groups was conducted. The identification of significant predictive variables from the regressions also allowed a reduction in the number of variables input into subsequent maximum likelihood and neural network classifications. A maximum of 16 input channels could be handled by the neural network algorithm, while maximum likelihood classifiers often perform best when trained with a limited number of discriminating channels (see below). Given the total number of available variables was 41, the regression results aided in reducing the number input to these classifiers.

In damage classification, for comparison with the other classifiers, 10 training/reference sets were selected from the original 100 trials and checked to ensure that they represented the full range of models in those trials.

3.1.2. Linear discriminant analysis

Linear discriminant analysis seeks $k - 1$ discriminant functions, where k is the number of classes to differentiate. These functions are linear combinations of the predictor variables that give the greatest amount of squared difference between groups relative to the variance within groups. Each class mean (centroid) in $k - 1$ dimensional space is determined. Observations are assigned to the class whose discriminant function has the smallest Mahalanobis distance to the class mean (Lachenbruch, 1975). In two-dimensional space (where $k = 3$ classes), the Mahalanobis distance is identical to the Euclidean distance. Stepwise discriminant analysis was performed using the same probabilities for entry and removal as the stepwise regression analysis. All available normally distributed spectral and environmental data were entered as independent variables into the analysis.

3.1.3. Maximum likelihood

Before running the maximum likelihood classifier, variable selection was carried out to eliminate redundant information contained in multiple discriminating variables (Mather, 1999; Piper, 1992). Sixteen significant discriminating variables were identified in the stepwise regression analysis. Of these, the five variables that accounted for maximum variance in the original data, determined through principal components analysis, were selected for input to the maximum likelihood classification. These included post-storm spectral band 3, pre-/post-storm ratios of TM bands 3 and 5, and freezing precipitation. Transformed proximity to forest edge was also included based on results from the regression analysis. The number of discriminating variables (5) exceeded Piper's (1992) recommendation of one variable per 10–30 observations for the low damage class, which contained between 12 and 17 observations.

3.1.4. Neural network

A simple back propagation neural network (Atkinson & Tatnall, 1997; Pao, 1989) was used that consisted of an input layer, one hidden layer and an output layer. Separate neural networks were trained for 40 sets of training/reference data, 20 sets using plot-based, and 20 sets using block-based stratification (see below). The maximum number of channels that could be handled by the algorithm was used, consisting of 11 TM spectral bands and band transformations determined to be significantly predictive of damage from the stepwise regression analysis, and all available environmental data. While neural networks can approximate any function type, selection of input variables was based on linear data reduction techniques for simplicity. For all trials, default parameters in the PCI algorithm were used: 1000 iterations, learning rate of 0.1 (controls the step size when weights are iteratively adjusted), momentum rate of 0.9 (refers to the size of the step at each iteration), maximum individual class error of 0.001, maximum total error of 0.01 (PCI Geomatics Group, 2001).

3.2. Stratification methods

From the total set of 104 plots with complete coverage of all of the above-mentioned geospatial data types, mutually exclusive training and reference samples were randomly generated for classification and accuracy assessment using multiple cross-validation trials (Efron & Tibshirani, 1993). An approximate 80/20% ratio of training to reference data was used for stratification on both plot and block bases. In the case of plot-based stratification, 100 separate samples of training and reference data were generated with this ratio for treatment of damage as a continuous variable (% crown loss) in the stepwise regression analysis (Table 2). Following this analysis, 10 of these samples were selected to compare among classification methods for treatment of damage as an ordinal variable (i.e. the three classes). In both of these analyses, randomly selected training and

Table 3
Regression model errors for 100 cross-validation trials

	R^2	S.E.	Reference RMSE
Minimum	0.24	13.7	12.6
Maximum	0.52	16.9	25.0
Mean	0.39	15.3	18.2
S.D.	0.065	0.7	2.5

Units of S.E. and RMSE are percent crown loss.

reference data plots could be in close proximity to each other since each block was comprised of four adjacent plots. Spatial proximity between plots was expected to produce artificially high classification accuracies due to the effects of spatial autocorrelation already discussed, registration errors and the point spread function of the TM sensor, which integrates reflectance over a larger area than the pixel bounds. To evaluate spatially independent training and reference data, an additional 20 samples were generated using block-based stratification with 5 blocks (20 plots) set aside as reference data. From the above three datasets and analyses, the effects of spatial proximity on classification accuracy were assessed as described in Section 3.3.

3.3. Accuracy assessment

Classification accuracy was determined using three reference data types. The first was a comparison of the classification to the training data used to develop it. This method over-estimates true classification accuracy but is a useful means for comparison of multiple classification trials using different input data, parameters, or classifiers (as in this study). The second used plots randomly set aside as reference data in each trial. As these reference plots were almost always in close proximity to training plots taken from the same blocks, this method was expected to produce positively biased accuracy due to spatial proximity in the data. The third method used entire blocks as reference data. Blocks were generally spaced far apart from one another (typically more than 25 km) so these reference data were assumed to be spatially independent.

In regression modeling of percent crown loss, the root mean square error between the predicted and actual values was examined for both training, and reference sets for all 100 trials. For training data, this error is the standard error (S.E.) of regression, while for independent reference data, it is reported as the root mean square error (RMSE).

Table 4
Regression model errors grouped according to common predictor variables

Model group	Significant predictors	N	S.E.	Reference RMSE
1	B1_pre, B5_pre, Edgeprox	33	14.9	18.0
2	B3_post, Edgeprox	19	15.1	16.4
3	B3_Ratio, Edgeprox	10	16.2	18.0
4	B7_post, Edgeprox	13	15.7	18.4
5	Other, Edgeprox	25	15.5	19.9

Pre=pre-storm, Post=post-storm, Ratio=ratio of pre- to post-storm spectral band, Edgeprox=proximity of plot to nearest forest edge.

Ordinal classification errors are reported as the user's accuracy (100% – % errors of commission), producer's accuracy (100% – % errors of omission), overall accuracy (total correct plots/total plots), and κ statistic (overall accuracy – accuracy achievable through random class assignment) (Lillesand & Kiefer, 1999). Overall accuracy within each classification and stratification method was calculated by summing the error matrices of all trials performed within the classification and stratification method. Differences among classification accuracies were assessed using pairwise t -tests, with each pair consisting of a reference set classification accuracy obtained using different classifiers. Difference distributions were visually assessed for normality.

4. Results

4.1. Damage as a continuous variable: linear regression models

All 100 regression models were significant at $P < 0.0005$ and had standard errors between 13.7% and 16.9% crown loss (Table 3). The range of RMSE of the reference datasets was greater than the range of standard errors, having both lower minimum and higher maximum errors. The mean error for the reference sets was 2.9% crown loss higher than the mean standard error. This difference was due to regression minimizing the residual sum of squares between actual and predicted values. The error generated from the reference sets is a more realistic estimate of true model error when applied to the whole geospatial dataset.

While the total error was relatively constant among the 100 trials, there was some variability due to the different significant predictors selected by the stepwise regressions (Table 4). Of the 100 models, 75 could be grouped according to 1 of 4 sets of significant predictors (model groups 1–4 in Table 4). These predictors were common to all regressions in the model group, while other variables not listed were either entered subsequently or were not common to all models of that group. Proximity to forest

Table 5
Overall training data classification accuracies—the most accurate training data classification is shown in bold

Training set #	Regress	Discrim	Max likelihood	Neural net
1	62%	70%	76%	96%
2	53%	60%	70%	99%
3	56%	64%	72%	97%
4	53%	66%	73%	98%
5	53%	62%	70%	100%
6	52%	51%	69%	99%
7	57%	65%	72%	91%
8	53%	58%	71%	92%
9	60%	59%	73%	75%
10	57%	65%	79%	94%
Average	55%	62%	72%	94%
Range	10%	19%	10%	25%

Table 6
Overall plot-based reference data classification accuracies—the most accurate reference data classification is shown in bold

Reference set #	Regress	Discrim	Max likelihood	Neural net
1	38%	38%	50%	50%
2	64%	64%	62%	85%
3	65%	62%	54%	54%
4	55%	45%	58%	63%
5	56%	44%	56%	69%
6	67%	61%	56%	67%
7	38%	52%	45%	67%
8	36%	64%	56%	67%
9	50%	45%	52%	60%
10	50%	41%	62%	76%
Average	51%	52%	55%	65%
Range	31%	26%	17%	35%

edge was automatically entered in all 100 models, suggesting that it is highly related to ice storm damage and complementary to spectral and other environmental data. Of the other environmental data, elevation was a significant predictor in only two models, while freezing precipitation was significant in four.

Pre-storm TM bands 1 and 5 were entered together 33 times and were therefore related to the susceptibility of forest species and structure to subsequent ice storm damage. These bands have been shown to be useful for forest type mapping and vegetation moisture content, which may affect forest susceptibility to ice storm damage (Hauer et al., 1994; Van Dyke, 1999). However, the relation between pre-storm blue reflectance and ice storm damage is difficult to explain, as this band is particularly sensitive to Rayleigh scattering (Lillesand & Kiefer, 1999). Post-storm band 3 and a pre/post-storm band 3 ratio were significant predictors a combined total of 29 times. Thirteen models entered post-storm TM band 7, while no more than 5 of the 25 remaining models could be grouped according to 1 or more common predictors.

Models that entered post-storm TM band 3 first had the lowest independent reference set errors, suggesting that perhaps this band is most useful for differentiating levels of damage. Post-disturbance TM band 3 has been

found to be useful for discriminating different levels of deciduous damage in at least one other study (Vogelmann & Rock, 1989). In another study by Vogelmann (1990), NDVI was determined to be suitable for distinguishing low, medium and high deciduous damage. This contrasts with results found here where none of the regression models entered the post-storm NDVI as the most significant predictor, but two models entered the pre-post-storm NDVI ratio first.

Based on results from the regression analysis, the following spectral variables were retained for classification using neural networks: pre-storm TM bands 1–3, 5, and 7, post-storm TM bands 3 and 7 and NDVI, ratios of pre- to post-storm reflectance for TM bands 1, 3, and 5, and all available environmental variables. The potential to identify non-linear patterns using neural networks justified the inclusion of environmental variables that were not linearly related to damage, while the selection of the spectral and edge proximity variables was based on linear variable reduction techniques.

4.2. Damage as an ordinal variable: classification comparison results

4.2.1. Training data accuracies

Table 5 presents the overall training data classifications accuracies of three damage levels using the four methods described above.

The 10 neural network classifications predicted the training dataset most accurately in all cases, achieving an overall accuracy of 94%. The maximum likelihood classifier did not perform nearly as well as the neural networks, with an overall accuracy of 72% for its 10 classifications. However, it performed most consistently, with training set accuracies ranging from 69% to 79%. Pairwise *t*-tests performed to assess the significance of differences among classification accuracies showed significantly different accuracies between all pairs of classifiers at $P < 0.01$. Both discriminant analysis and regression classifiers predicted training data poorly. Even with the typically inflated accuracies of training data over that expected from independent reference data, these results show that only the neural

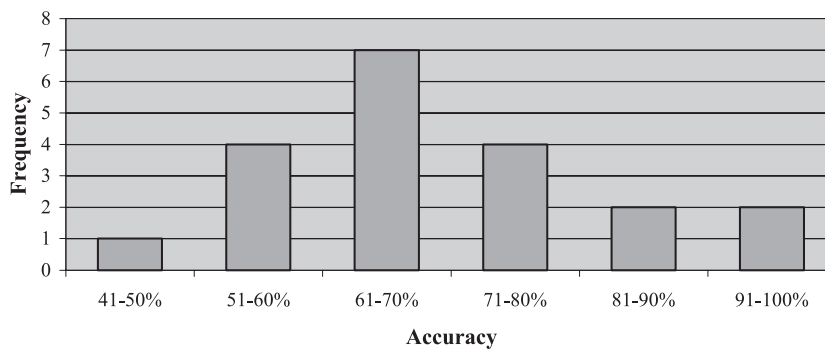


Fig. 2. Distribution of neural network damage classification accuracies from 20 cross-validation trials and plot-based stratification.

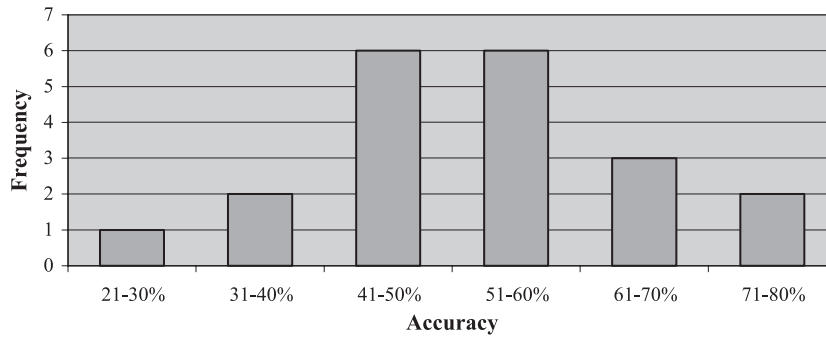


Fig. 3. Distribution of neural network damage classification accuracies from 20 cross-validation trials and block-based stratification.

network and maximum likelihood classifiers are useful for such damage classification.

4.2.2. Plot-based reference data accuracies

A direct comparison of the 10 plot-based reference data accuracies for the four classifiers again revealed the superiority of the neural network (Table 6). Its accuracies were highest seven out of 10 times, while its performance was tied for first 2 of the remaining three times. Only 1 of the 10 plot-based reference datasets had a lower overall accuracy than the other classifiers (trial #3). The range of classification accuracies was lowest for the maximum likelihood (17%) and highest for the neural network (35%) (Table 6). Pairwise *t*-tests performed among the classifiers showed that all produced non-significantly different accuracies, except for the neural networks, which were significantly better than the others ($P < 0.01$).

The distribution of neural network accuracies shown in Table 6 is approximately normal, however, 10 trials were insufficient to properly assess it. A second set of randomly split training and plot-based reference datasets were therefore generated and the classification results added to those of the first set to increase the number of trials to 20 (Table 2). The second set produced slightly higher accuracies than the first set, primarily due to two networks with accuracies greater than 90%. However, the difference between the two sets was determined to be insignificant using a *t*-test. Fig. 2 shows the distribution of accuracies for the combined 20 neural network classifications.

4.3. NN reference data accuracies using block-based stratification

Comparison of the accuracies of the block-based stratifications of training and reference data (Fig. 3) to the plot-based results of Fig. 2 revealed the inflationary effects of the spatial proximity between training and reference data in the plot-based assessment. Overall block-based accuracy for 20 sets was 54.5% with a κ of 0.25 (Table 7), which was 14.2% lower than the overall accuracy obtained from the 20 neural networks using plot-based stratification. Because neural networks learn training data exceptionally well, and because the plot-based reference data were spatially autocorrelated

with the training data, these reference data were essentially pseudo-replicates of adjacent training data, thereby producing inflated accuracy estimates.

Table 7 shows that while the overall classification accuracy was quite low, high damage areas were mapped relatively well. Indeed, 77.3% of spatially independent blocks having suffered high damage were correctly identified as such in the classifications. A 63.1% user’s accuracy for the high damage class suggests that 63.1% of blocks classified as severe damage were actually severely damaged. The low and moderate damage classes were subsequently merged into a single class to determine the accuracy with which high damage (significant probability of further decline) and low to moderate damage (low chance of further decline) could be classified. The overall accuracy increased to 69.3%, while the κ statistic improved to 0.39 with a standard deviation of 0.07, which was significantly different from chance agreement at $P < 0.0001$.

A map of the two deciduous forest ice storm damage classes was produced (Fig. 4) using a voting strategy to select the most frequently occurring class for the 20 neural network classifications at each pixel location (Kanellopoulos & Wilkinson, 1997). The frequency of the most often occurring class (the mode) at each location provided a measure of confidence for the mapped output on a per pixel basis.

The resulting map suggests that greater damage occurred close to forest edges and at higher elevations found in the northwestern portion of eastern Ontario. Damage does not appear to be directly related to precipitation, which was heaviest in the central to southeastern

Table 7
Combined error matrix for 20 neural network classifications, each assessed using 20 reference plots and block-based stratification

Classification	Reference damage class			Total	User’s
	1	2	3		
1	15	16	8	39	38.5%
2	43	63	33	139	45.3%
3	19	63	140	222	63.1%
Total	77	142	181	400	
Producer’s	19.5%	44.4%	77.3%		
κ	0.25			Overall	54.5%

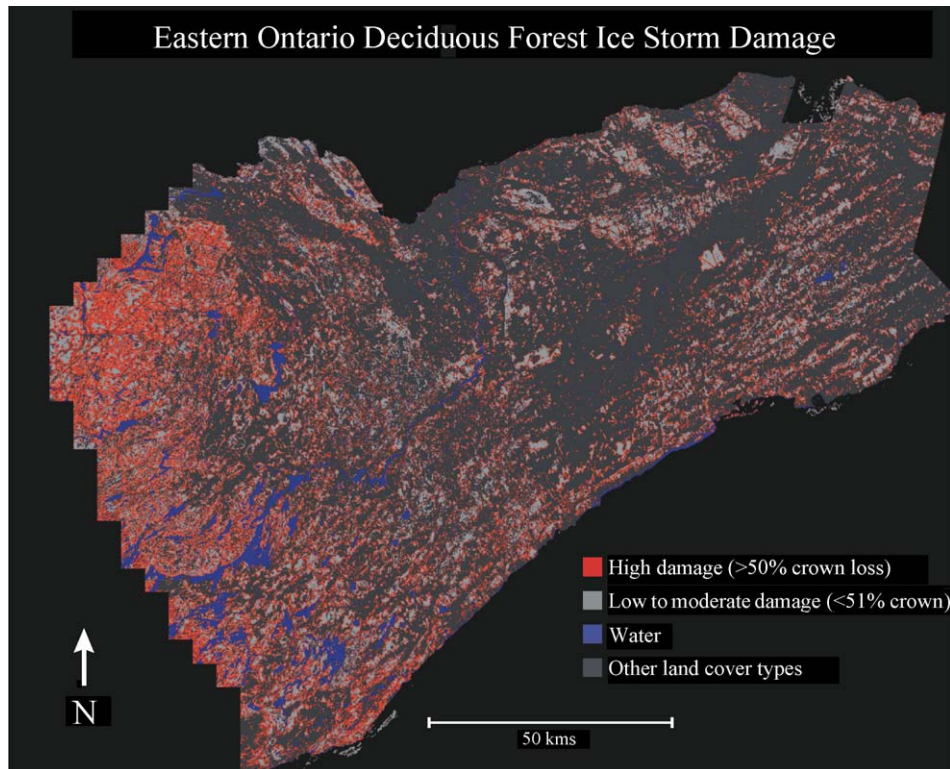


Fig. 4. Deciduous forest damage in eastern Ontario resulting from the January 4–10, 1998 ice storm.

parts of eastern Ontario. Factors that affect the magnitude of damage suffered from ice storm events are numerous, such as tree species, age and size, ice accretion, and stand position, among others (Proulx & Greene, 2001), but complete discussion of them is beyond the scope of this paper.

5. Discussion

Due to the relatively small number of deciduous damage mapping studies in the literature and the absence of published deciduous damage classification accuracies, comparison of results found here must be made primarily to studies of coniferous forest damage. In modelling damage as a continuous variable, Ekstrand (1994) obtained a correlation (r) of -0.75 ($P < 0.001$) between TM band 4 reflectance and conifer percent needle loss for 30 sites. The correlation coefficient improved to $r = 0.81$ for 39 sites when field and air photo determined stand characteristics were included in the model. In another study, Collins and Woodcock (1996) used orthogonal transformations of multitemporal and multispectral TM data. The best correlation coefficient obtained was $r = 0.89$ ($P < 0.0001$) for 25 mixed conifer sites using Kauth-Thomas change components. While all regression models in this study had an equal or lower correlation coefficient of $r = 0.72$ (Table 3), the significance level of all models was similar due to the larger sample sizes used in this study.

Damage classification typically requires assignment of a continuous damage measure into discrete damage classes. A limitation of the classification approach is that the boundaries between damage classes are artificial and subjective. For example, in this study, while a distinction is made between 24% crown loss and 26% crown loss in terms of damage classes, the difference between them is insignificant, especially in relation to the precision of visual crown loss estimation. Damage classes in this study were chosen to be consistent with those employed by other ice storm research groups, and to be able to assign a probability level of further decline from the literature based on the amount of crown loss suffered.

Lambert et al. (1995) provided an overview of nine previous satellite-based damage studies in coniferous forests that demonstrated the variability of methods and results obtained from nine different studies. TM bands 1, 3, 4, 5, and 7 have all been used to map conifer damage, as well as various ratios of these bands. However, most of the studies had inadequate sample size (8–22) to allow direct comparison to this study with two exceptions. Rosengren and Ekstrand (1988) used 92 stands to obtain an accuracy of 76% for four damage classes, while Lambert et al., used 243 stands and logit regression to map even-aged stand damage with an accuracy of 71–75% for three classes.

Franklin et al. (1995) achieved a best overall accuracy of 86% using discriminant functions to classify 21 coniferous plots into three defoliation classes. Multi-temporal TM indices were used to obtain this result, consisting of pre-

and post-disturbance Tasseled Cap (Kauth-Thomas) brightness, greenness, and wetness. The same plot data that were used to produce the discriminant functions were also used to assess the classification accuracy. Thus, the accuracy obtained in Franklin et al. is optimistic and a similar accuracy would not be achieved with an independent reference set, as was shown in this study. Average training set accuracy for the discriminant analysis in this study (Table 5) was not found to be as high as those obtained in Franklin et al.. However, they assessed defoliation in pure conifer stands and a relatively small sample size was used. Additionally, the range of accuracies of 48–86% was wider than the range found here and the minimum accuracy was less than that of this study.

Franklin et al. (1995) also evaluated supervised and modified unsupervised k-means classifications using the 21 sites mentioned above, producing an overall training data accuracy of 67% for both methods. In this study, an average training set accuracy of 72% was achieved using a maximum likelihood classification (Table 5). This dropped to 55% when assessed using the 10 independent plot-based reference sets, with a best overall accuracy of 62% for a single classification (Table 6).

The overall accuracy obtained using neural networks and plot-based stratification in this study was similar to those obtained by Ardo et al. (1997) when using single date TM and topographic data to classify three conifer damage classes (62–68% overall classification accuracy). However, their results improved when using bi-temporal TM and topographic data (77–78% accuracy). The block-based stratification of data produced lower overall accuracies than the plot-based stratification for the neural network classifier. This was due to the high accuracy with which neural networks classify training data, and the effect of spatial proximity between training and reference plots. Block-based stratification was not performed with the other classifiers as none performed well enough in the plot-based stratification to consider further. However, the inflationary effects of spatial autocorrelation on accuracy of other classifiers will depend on how well the classifier predicts training data. Poorer classification of training data will likely result in less inflated accuracy of spatially proximal reference data. These results demonstrate the importance of spatial independence between training and reference data for proper validation. Few studies report distance between training and reference data or consider its effects on model accuracy.

Better overall classification accuracy may have been achievable had several neural network architectures been tested (e.g., different momentum and learning rates, number of hidden layers, number of iterations). A lack of consistent guidelines on network configuration led us to choose a basic architecture for evaluation. In addition, other input variables could be included depending on availability. For example, forest species and structure or forest management methods may be linked to damage. Inclusion of these was intended for this study but such data had not been collected for the

OMNR plots and forest inventory for eastern Ontario was too out of date.

Although neural networks performed better than other classifiers in this study, they have not been commonly applied in operational mapping due to perceived difficulties in extension of well learned training data over regional areas and in the time required to train the network and test different configurations. In this research, rigorous assessment of a high and low damage classification using spatially independent test data has shown that accuracy is reasonable for the whole eastern Ontario region. A set of 10 networks required only 2 days to train and use of neural networks enabled testing of more variable types than was possible with the parametric classifiers. Thus, for the purpose of this study, to produce a more precise and objective damage map than was obtained immediately following the storm using aerial sketch mapping, the methods have proven to be moderately successful.

The final map produced from the research is not intended to replace sketch mapping as a means for near real-time assessment, as Landsat data must be acquired in the growing season following such a storm and the environmental data require a certain period of time to integrate into the database. It can, however, in conjunction with the knowledge gained from the study, be used over the longer term in policy development for improved forest and landscape management to reduce susceptibility to future storms. After future storms, the methods can be applied to provide damage maps in the medium term (by the end of the summer following the storm) to supplement sketch maps and be used for insurance and salvage/restoration needs.

6. Conclusions

Modelling and classification of forest ice storm damage was conducted using Landsat and environmental data. This study sought to examine some of the variation in damage mapping error associated with (1) modeling or classification methods and (2) stratification methods of available plot data into training and reference sets. In comparison of classifiers, a simple neural network outperformed three parametric classifiers and compared favorably with results reported in other studies. Among the other classification methods selected for comparison, the range of accuracies obtained generally agreed with results from other studies where similar methods were used. The neural networks had difficulty discriminating low and moderate damage, but produced reasonable accuracies for high damage areas. The map that was produced using voting strategies could therefore be considered useful for targeting areas for cleanup and compensation to maple syrup producers where high damage was most likely to have occurred.

In data stratification for training and validation, the distance between training and reference data must be considered when assessing classification accuracy to ensure

spatial independence. Single training and reference sets can produce significantly biased classification accuracy, with the magnitude of bias being dependent on the classification method used. In order to obtain robust and representative classification accuracies, multiple trials should be performed and assessed using random subsets of data.

Acknowledgements

We thank Cathy Nielsen, Geoff McVey, John Winters, Peter Neave, Dave Bland, and Dendron Resource Surveys for their support. Funding for this project has been provided under the Canada-Ontario Agreement for the Ice Storm Economic Recovery Assistance Program, Annex A, Assistance for the Agricultural Sector, and Rural Communities in Eastern Ontario. This program is jointly funded by the Government of Canada and the Government of Ontario. Additional scholarship and grant funding was provided by the Natural Sciences and Engineering Research Council of Canada (NSERC) to I. Olthof and D. King.

References

- Ardo, J., Pelesjo, P., & Skidmore, A. (1997). Neural networks, multitemporal Landsat Thematic Mapper data and topographic data to classify forest damages in the Czech Republic. *Canadian Journal of Remote Sensing*, 23, 217–230.
- Atkinson, P. M., & Tatnall, A. R. L. (1997). Neural networks in remote sensing. *International Journal of Remote Sensing*, 18, 699–709.
- Carter, G. A. (1993). Responses of leaf spectral reflectance to plant stress. *American Journal of Botany*, 80, 239–243.
- Chen, J. M., & Leblanc, S. G. (1997). A four-scale bi-directional reflectance model based on canopy architecture. *IEEE Transactions on Geoscience and Remote Sensing*, 35, 1316–1337.
- Collins, W. E. (1978). Remote sensing of crop type and maturity. *Photogrammetric Engineering and Remote Sensing*, 44, 43–55.
- Collins, J. B., & Woodcock, C. E. (1996). An assessment of several linear change detection techniques for mapping forest mortality using multitemporal Landsat TM data. *Remote Sensing of Environment*, 56, 66–77.
- Coons, C. F. (1999). *Effect of ice storm damage and other stressors on sugar bush health and sap productivity—literature review and synthesis*. Eastern Ontario Model Forest Information Report. 77 pp.
- Efron, B., & Tibshirani, R. J. (1993). *An introduction to the Bootstrap*. New York: Chapman & Hall, 436 pp.
- Ekstrand, S. (1994). Assessment of forest damage with Landsat TM: Correction for varying forest stand characteristics. *Remote Sensing of Environment*, 47, 291–302.
- Franklin, S. E., Waring, R. H., McCreight, R. W., Cohen, W. B., & Fiorella, M. (1995). Aerial and satellite sensor detection and classification of western spruce budworm defoliation in a subalpine forest. *Canadian Journal of Remote Sensing*, 21, 299–308.
- Friedl, M. A., Woodcock, C., Gopal, S., Muchoney, D., Strahler, A. H., & Barker-Schaaf, C. (2000). A note on procedures used for accuracy assessment in land cover maps derived from AVHRR data. *International Journal of Remote Sensing*, 21, 1073–1077.
- Gates, D. M., Keegen, H. J., Schleter, J. D., & Weidner, V. R. (1965). Spectral properties of plants. *Applied Optics*, 4, 11–20.
- Hauer, R. J., Hruska, M. C., & Dawson, J. O. (1994). *Trees and ice storms: The development of ice storm-resistant urban tree populations*. Department of Forestry. University of Illinois at Champaign, Urbana, III. Spec. Publ. 94-1.
- Holben, B. N., Tanre, D., Buis, J. P., Setzer, A., Vermote, E., Reagan, J. A., Kaufman, Y. J., Nakajima, T., Lavenue, F., Jankowiak, I., Smirnov, A., Eck, T. F., & Slutsker, I. (1998). AERONET—A federated instrument network and data archive for aerosol characterization. *Remote Sensing of Environment*, 66, 1–16.
- Hopkin, A. A., Williams, T., Sajan, R., Pedlar, J., & Nielsen, C. (2003). Ice storm damage to Eastern Ontario forests: 1998–2001. *Forestry Chronicle*, 79, 47–53.
- Horler, D. N. H., Barber, J., & Barringer, A. R. (1980). Effects of heavy metals on the absorbance and reflectance spectral of plants. *International Journal of Remote Sensing*, 1, 121–136.
- Kanellopoulos, I., & Wilkinson, G. G. (1997). Strategies and best practices for neural network image classification. *International Journal of Remote Sensing*, 18, 711–725.
- Kidon, J., Fox, G., McKenney, D., & Rollins, K. (2001). Economic impacts of the 1998 ice storm on the eastern Ontario maple syrup industry. *Forestry Chronicle*, 77, 667–675.
- Lachenbruch, P. A. (1975). *Discriminant analysis*. New York: Hafner Press, 128 pp.
- Lambert, N. J., Ardo, J., Rock, B. N., & Vogelmann, J. E. (1995). Spectral characterization and regression-based classification of forest damage in Norway spruce stands in the Czech Republic using Landsat Thematic Mapper data. *International Journal of Remote Sensing*, 16, 1261–1287.
- Latifovic, R., Cihlar, J., & Beaubien, J. (1999). Clustering methods for unsupervised classification. *Proceedings of the 21st Canadian Remote Sensing Symposium, II-509-II-515 June, Ottawa, Canada*.
- Lautenschlager, R. A., & Nielsen, C. (1999). Ontario's forest science efforts following the 1998 ice storm. *Forestry Chronicle*, 75, 633–641.
- Lemon, P. C. (1961). Forest ecology of ice storms. *Bulletin of the Torrey Botanical Club*, 88, 21–29.
- Lévesque, J., & King, D. J. (2003). Spatial analysis of radiometric fractions from high-resolution multispectral imagery for modelling forest structure and health. *Remote Sensing of Environment*, 84, 589–602.
- Lillesand, T. M., & Kiefer, R. W. (1999). *Remote sensing and image interpretation* (4th ed.). New York: Wiley, 750 pp.
- Mageau, M. T., Costanza, R., & Ulanowicz, R. E. (1995). The development and initial testing of a quantitative assessment of ecosystem health. *Ecosystem Health*, 1, 201–213.
- Mather, P. M. (1999). *Computer processing of remotely-sensed images: An introduction* (2nd ed.). New York: Wiley, 292 pp.
- McKay, G. A., & Thomson, G. A. (1969). Estimating the hazard of ice accretion in Canada from climatological data. *Journal of Applied Meteorology*, 8, 927–935.
- Milton, J., & Bourque, A. (1999). *A climatological account of the January 1998 ice storm in Quebec*. Environment Canada, Quebec Region Report CES-Q99-01, Hull, Quebec, 87 pp.
- Olthof, I., & King, D. J. (2000). Development of a forest health index using multispectral airborne digital frame camera imagery. *Canadian Journal of Remote Sensing*, 26, 166–176.
- Ontario Ministry of Natural Resources (OMNR) (1997). Bioindicators of forest health and sustainability. *Forest Research Information Paper*, ISSN 1319-9118; no. 138. 101 pp.
- Pao, Y. H. (1989). *Adaptive pattern recognition and neural networks*. Reading, MA: Addison-Wesley Publishing, 309 pp.
- PCI Geomatics Group (2001). *PCI Geomatica software package, version 8.0*. Richmond Hill, ON: PCI Geomatics Group.
- Pellikka, P. K. E., Seed, E. D., & King, D. J. (2000). Modelling deciduous forest ice storm damage using CIR aerial imagery and hemispheric photography. *Canadian Journal of Remote Sensing*, 26, 394–405.
- Piper, J. (1992). Variability and bias in experimentally measured classifier error rates. *Pattern Recognition Letters*, 13, 685–692.
- Proulx, O. J., & Greene, D. F. (2001). The relationship between ice thickness and northern hardwood tree damage during ice storms. *Canadian Journal of Forest Research*, 31, 1758–1767.

- Quebec Ministry of Natural Resources (QMNR) (2000). *Management of ice storm damaged stands*, ISBN: 2-550-35993-3. 65 pp.
- Radeloff, V. C., Mladenoff, D. J., & Boyce, M. S. (1999). Detecting jack pine budworm defoliation using spectral mixture analysis: separating effects from determinants. *Remote Sensing of Environment*, 69, 156–169.
- Rock, B. N., Vogelmann, J. E., & Defeo, N. J. (1989). The use of remote sensing for the study of air pollution effects in forests. *Biologic markers of air-pollution stress and damage in forests* (pp. 183–194). Washington, DC: National Academy Press.
- Rosengren, M., & Ekstrand, S. (1988). A method aiming at monitoring of large-area forest decline using satellite imagery. *Proceedings-Seminar on remote sensing of forest decline attributed to air pollution, April 1987, Laxenburg, Austria* (pp. 1–20).
- Scarr, T. A., Hopkin, A. A., & Howse, G. M. (2003). Aerial sketch-mapping of the 1998 ice storm in Eastern Ontario. *Forestry Chronicle*, 79, 91–98.
- Seed, E. D., & King, D. J. (2003). Shadow brightness and shadow fraction relations with effective leaf area index: Importance of canopy closure and view angle in mixedwood boreal forest. *Canadian Journal of Remote Sensing*, 29, 324–335.
- Singhroy, V. (1995). Spectral characterization of vegetation at mine tailings. *Proceedings of the Sudbury 95 mining and the environment—An integrated approach to planning and rehabilitation for the 21st century, 28 May–1 June 1995, Sudbury, Ontario* (pp. 193–197).
- Treitz, P. M., Howarth, P. (1996). *Remote sensing for forest ecosystem characterization: a review*. Natural Resources Canada, Can. For. Serv., Sault Ste. Marie, Ontario. NODA/NFP Technical Report TR-12, 51 pp.
- Van Dyke, O. (1999). *A literature review of ice storm impacts on forests in Eastern North America*. SCSS Technical Report 112, 33 p.
- Vermote, E. F., Tanré, D., Deuzé, J. L., Herman, M., & Morcrette, J. J. (1997). Second simulation of the satellite signal in the solar spectrum, 6S: An overview. *IEEE Transactions on Geoscience and Remote Sensing*, 35, 675–686.
- Vogelmann, J. E. (1990). Comparison between two vegetation indices for measuring different types of forest damage in the north-eastern United States. *International Journal of Remote Sensing*, 11, 2281–2297.
- Vogelmann, J. E., & Rock, B. N. (1989). Use of Thematic Mapper data for the detection of forest damage caused by the pear thrips. *Remote Sensing of Environment*, 30, 217–225.
- Yuan, X., King, D. J., & Vlcek, J. (1991). Sugar maple decline assessment based on spectral and textural analysis of multispectral aerial videography. *Remote Sensing of Environment*, 37, 47–54.